Mode characteristics of metal-coated microcavity

Jinyi Gu,[1] Zhuo Zhang,[1] Mi Li,[1] and Yuejiang Song[1,2,*]

[1]*Institute of Optical Communication Engineering, Nanjing University, Nanjing 210096, China*

[2]*Beckman Laser Institute, University of California, Irvine, Irvine, California 92612, USA*

(Received 13 April 2014; published 14 July 2014)

The mode characteristics (dispersion relation and Q factor) of metal-coated microcylinders are achieved from the analytical resonance eigenequation. Among the resonance modes, two surface plasmon polariton (SPP) modes have completely different characteristics compared to the hybrid plasmonic whispering gallery modes (WGMs). In the metal-coated microcylinder, the Q factor of the asymmetrical SPP mode can be greater than the symmetric mode, and the hybrid plasmonic WGMs have a greater mode index range, extending down to zero. Also, the mode indexes and Q factors of the resonance modes are measured by the attenuated total reflection and resonance linewidth method, respectively. The experimental results agree well with the theoretical.

DOI: 10.1103/PhysRevA.90.013816 PACS number(s): 42.60.Da, 42.79.−e, 73.20.Mf

I. INTRODUCTION

The dielectric microcavity has been receiving great attention for many years due to its high Q factor and small mode volume [1–3]. It has been utilized in a variety of applications, such as biochemical sensor [4,5], low threshold laser [6–8], and nonlinear conversion [9,10]. Recently, the metal-coated microcavity has also been studied for its unique hybrid characteristics of both whispering gallery mode (WGM) and surface plasmon polariton (SPP): It has a relatively high Q factor of WGM and optical amplitude enhancement as well as small mode volume of SPP [11–15], which may have great potential applications. In recent experimental research, high-Q-factor plasmonic WGMs have been verified and measured in sa ilver-coated microdisk [11] and microbottle resonator [14]; also, theoretical calculation has also predicted the high Q factor in the metal-coated microtoroid [13] or hollow silver tube [15]. At the same time, SPP modes of metal microcavity have been studied in both theory and application, such as in SPP laser [16] and SPP resonance [17].

In this paper, we comprehensively study the mode characteristics of a metal-coated microcylinder as a function of microcylinder radius and metal film thickness. Through its analytical eigenequation, the mode dispersion and Q factor can be achieved through numerical calculation. The plasmonic WGMs exhibit interesting characteristics for both the mode index and Q factor. Both symmetric and asymmetric SPP modes are completely different from the hybrid plasmonic WGMs and are experimentally demonstrated in metal-coated microcavity. The Q factor of an asymmetrical SPP mode can be higher than that of a symmetric SPP mode. The hybrid plasmonic WGMs have a wide mode index range and their mode indexes can range down to zero. The mode index and Q factor are measured through attenuated total reflection (ATR) and resonance linewidth methods, respectively, which agrees well with the theoretical predictions.

II. THEORETICAL MODE CHARACTERISTICS

In this paper a cylindrical microcavity, a silver-coated microcylinder is used for the study; its schematic profile is shown in Fig. 1(a). The metal-coated fiber microcylinder is comprised of three layers of materials: the inner cylindrical fiber of radius R and index n_i, the medial metal film of thickness d and index n_{me}, and the outer cladding medium of semi-infinite dimension and index n_o. The outer medium discussed in this paper is air. The metal-coated fiber microcylinder is fabricated by evaporating silver onto the surface of the fiber microcylinder. The fiber microcylinder is prepared by etching the commercial single mode fiber in HF solution to the desired size. Then the prepared microcylinder is coated uniformly with silver film by thermally evaporating silver onto its surface while rotating around its longitudinal axis. The thickness of metal film can be monitored by the oscillation quartz in the evaporation machine, and be controlled by the evaporation rate and time. The optical micrograph of one silver-coated microcylinder sample is shown in Fig. 1(b); the uniform silver film is assured by the scanning electron microscope (SEM) image, and its thickness is approximately 67 nm, as shown in Fig. 1(c).

The metal-coated microcylinder can be treated as the three layers of WGM microcavity, and its mode eigenequation can be derived from the boundary conditions [5,18]. The cylindrical coordinate is used for the microcylinder cavity. Transverse magnetic (TM) [transverse electric (TE)] mode designates that only the axial field component, H_z (E_z), of the three magnetic (electric) field components, is nonzero. The resonance mode can be designated as (p, m, l), where p is the transverse magnetic or transverse electric polarization, m is the azimuthal mode number, and l is the radial mode number. For example, the amplitude of resonance mode (TM mode) in the radial direction can be derived as

$$\frac{n_i J_m(kn_{me}R_i)J_m'(kn_iR_i) - n_{me}J_m(kn_iR_i)J_m'(kn_{me}R_i)}{n_o J_m(kn_{me}R_o)\left[H_m^{(1)}(kn_oR_o)\right]' - n_{me}H_m^{(1)}(kn_oR_o)J_m'(kn_{me}R_o)} = \frac{n_i H_m^{(1)}(kn_{me}R_i)J_m'(kn_iR_i) - n_{me}J_m(kn_iR_i)\left[H_m^{(1)}(kn_{me}R_i)\right]'}{n_o H_m^{(1)}(kn_{me}R_o)\left[H_m^{(1)}(kn_oR_o)\right]' - n_{me}\left[H_m^{(1)}(kn_{me}R_o)\right]'H_m^{(1)}(kn_oR_o)},$$

where J_m and $H_m^{(1)}$ are the mth Bessel function and Hankel function of first kind, respectively. $R_i = R$ and $R_o = R + d$ are the inner and outer radii of the metal film of the

*yjsong@nju.edu.cn

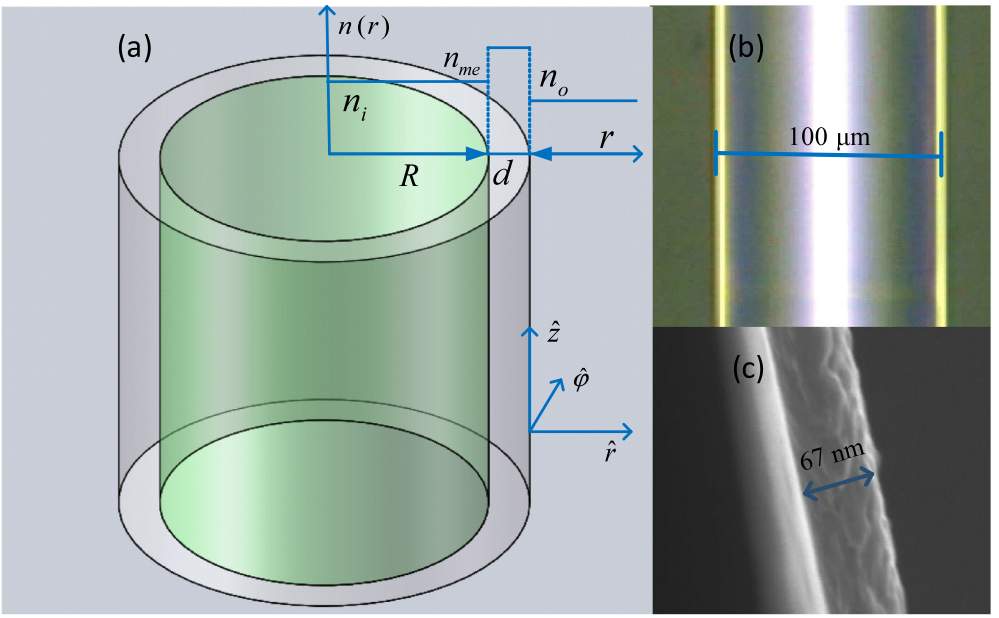

FIG. 1. (Color online) Schematic profile (a) and optical micrograph (b) of metal-coated microcylinder, and SEM image (c) of the metal film. R is the radius of fiber microcylinder; d is the thickness of metal film; n_i, n_{me}, and n_o are the refractive index of inner microcylinder, medial metal film, and outer medium, respectively.

metal-coated microcylinder, respectively. k is the complex eigen-wave-number in the vacuum, and can be calculated from the above eigenequation.

From the modal eigenequation, the dispersion relation and Q factor can be directly calculated from the complex resonance wave number k, according to the relationships $n = m/[\mathrm{Re}(k)R]$ and $Q = \mathrm{Re}(k)/[2\mathrm{Im}(k)]$, where $\mathrm{Re}(k)$ and $\mathrm{Im}(k)$ are the real part and imaginary part of complex k, respectively. These two characteristics are dependent on both the radius of the microcylinder and the thickness of the metal film. We first calculate the dispersion relation and Q factor as a function of radius R of the fiber microcylinder. In the calculation, we suppose the resonance wavelength is within the 65-nm wave band and no material dispersion is considered in this narrow wave band. In this case, the resonance mode (p, m, l) can also be simplified as TM l or TE l, for convenience. The indexes n_i, n_{me}, n_o of the inner fiber, silver film, and outer air are 1.4565, $0.0245 + 4.7635i$, and 1.0000, respectively, in the 65-nm wave band. The thickness of the silver film is fixed at $d = 67$nm, which corresponds to the experimental size. The dispersion relation and Q factor of plasmonic WGMs are calculated in Fig. 2. Also, the field intensity and amplitude distributions in the radial direction are calculated for some typical modes in Fig. 3.

TM modes (solid line) and TE modes (dashed line) have totally different characteristics in the SPP mode in Fig. 2. TM modes exhibit two SPP modes localized near the surfaces of the metal film, but TE modes do not. Indeed, SPP modes can be considered as the special WGM (TM, m,0) with radial mode number $l = 0$, where the maximum field amplitude is on the surface of the metal film. There are two different types of SPP modes, the SPPa and SPPs modes. The SPPa mode's index increases with the decreasing of the radius R, and has a minimum value of 1.5290 when R becomes infinite. Most of the intensity of the SPPa mode is localized near the inner metal

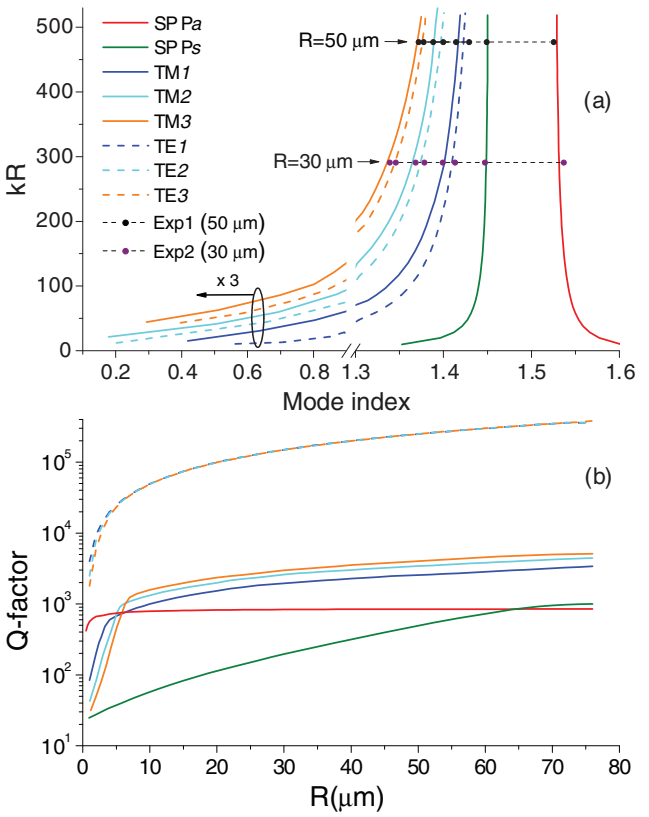

FIG. 2. (Color) The dispersion relations (a) and Q factor (b) as a function of the radius R of the microcylinder. The resonance wavelength is in the 650-nm wave band; k is the wave number of the resonance wavelength. The thickness of silver film is 67nm; the indexes of inner fiber, medial silver film, and outer air are 1.4565, $0.0245 + 4.7635i$, and 1.0000, respectively. Material dispersion is not considered in the resonance wave band.

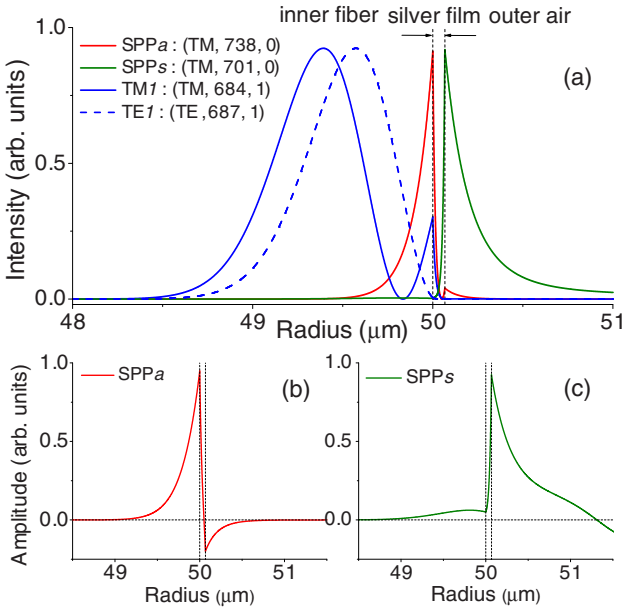

FIG. 3. (Color online) The intensity ($|H_z|^2$ for TM mode or $|E_z|^2$ for TE mode) and amplitude distributions in the radial direction of some typical modes. (a) The intensity distribution of SPP*a*, SPP*s*, TM1, and TE1 modes; (b), (c), the amplitude distribution of SPP*a* and SPP*s* modes, respectively. Here, the metal-coated microcylinder is composed of a 50-μm radius fiber microcylinder, a 67-nm silver film, and outer air.

surface [see Fig. 3(a)], and the SPP*a* mode is the asymmetrical mode due to the opposite sign of field amplitudes at both dielectric-metal interfaces [see Fig. 3(b)]. The SPP*s* mode has different characteristics compared to the SPP*a* mode: Its index decreases with the decreasing of R, and has a maximum value of 1.4500. The mode index of the SPP*s* mode is always less than that of the SPP*a* mode. The intensity of the SPP*s* mode is primarily located in the outer surface of the metal film, and it is the symmetrical mode due to the same sign of optical amplitudes at the both interfaces [see Fig. 3(c)]. Compared with all other modes, the SPP*s* mode is the extraordinary mode, as it can exhibit the guided mode or surface mode depending on its mode index [19,20]. Here, differing from the SPP*a* mode, the field of the SPP*s* mode in the inner fiber microcylinder is not a surface plasmon wave but a pure WGM, due to the huge index contrast between the inner fiber and outer air. Nevertheless, the SPPs mode is a SPP mode, essentially, because most of its intensity is still localized in the outer surface plasmon wave.

Meanwhile, the SPP*a* and SPP*s* modes have different Q factor characteristics. As shown in Fig. 2(b), the Q factor of SPP*a* mode is nearly constant from 567 to 846, but the Q factor of the SPP*s* mode increases dramatically from 25 to 714 when the radius R increases from 1 to 60 μm. When the radius becomes smaller, the Q factor of the SPP*a* mode is not seriously degraded because the field of the SPP*a* mode can be tightly localized in the inner fiber microcylinder due to small mode volume. But, for the SPP*s* mode, its field will radiate more into the air, so the Q factor decreases quickly due to radiation loss and metal absorption loss. When R is less than 64 μm, the Q factor of the SPP*a* mode is greater than that of the SPP*s* mode, which is different from long-range SPP in a one-dimensional metal slab waveguide [21]. But if the radius becomes larger, the Q factor of the SPP*s* mode is greater than that of the SPP*a* mode, and it will approach its maxima gradually.

Besides two special SPP modes ($l = 0$), both TM and TE guided modes ($l = 1, 2, 3\ldots$) are hybrid plasmonic WGMs, whose maximum field amplitude is in the inner fiber microcylinder and not on the metal film surface [see Fig. 3(a)]. Also the field amplitude of the TM mode is enhanced near the metal surface, but the TE mode is not enhanced due to the TM characteristics of the SPP mode. In Fig. 2(a), the mode indexes decrease with the decreasing of the radius R, and may approach zero, because the hybrid WGMs can be restrained towards the fiber axis and prevented from serious radiating by metal film even when R is very small. Similar results have been shown in a one-dimensional metal-clad waveguide [20,22]. Thus, a metal-coated microcavity has a wider mode index range than a dielectric microcavity. Each mode has its corresponding cutoff radius, which means that there is the minimum radius for supporting a certain mode. For the same l, the index of the TE mode is always greater than the TM mode. In Fig. 2(b), for the larger radius (>10 μm), the Q factors of the TE modes ($l = 1, 2, 3$) are almost the same (relative error less than 1%), and increase almost linearly with the radius R with the slope of $\sim 5025/\mu$m. But for the TM modes, their Q factors increase nonlinearly with R, and the Q factor of high-l mode is greater than of low-l mode. But for the small radius (<5 μm), the higher-l modes (for both TE and TM modes) have the lower Q factors, because the high-l mode will suffer from more absorption and radiation loss because it will penetrate more power into the metal film and air. When R is 50 μm, the Q factor of TM1, TM2, and TM3 is 2560, 3415, and 4050, respectively. But the Q factor of all three TE l modes is ~249 000, about two orders of magnitude greater than that of TM modes. The Q factor of the TE mode is always much higher than the TM mode because the TM mode has more loss than the TE mode due to SPP excitation.

Also we calculate the dispersion relation and Q factor of hybrid modes under different thickness of metal film while fixing the radius R. Here R is fixed at 30 μm, and the other parameters are the same as above. As shown in Fig. 4(a), two SPP modes have different characteristics of mode index compared to other modes. The mode index of the SPP*a* mode increases with the decreasing of silver film thickness d, but the index of the SPP*s* mode decreases with the decreasing of silver thickness. The other hybrid modes have the below dispersion characteristics: TE modes have a larger index than TM modes with the same l: For the same polarization mode, the higher the radial mode number l, the smaller the mode index; the mode index increases gradually with the decreasing of silver thickness. However, when d is very thin (<20nm), the index will increase greatly due to the strong coupling interactions of the fields on both metal film surfaces. And in Fig. 4(b), the Q factor of the SPP*a* mode increases with the thickness of the metal film and then approaches its maxima ~900. Instead, the Q factor of SPP*s* decreases with the thickness of silver film, and then approaches its minima ~155. When d is 41nm, SPP*s* and SPP*a* modes have the same Q factor of 531. The Q factor

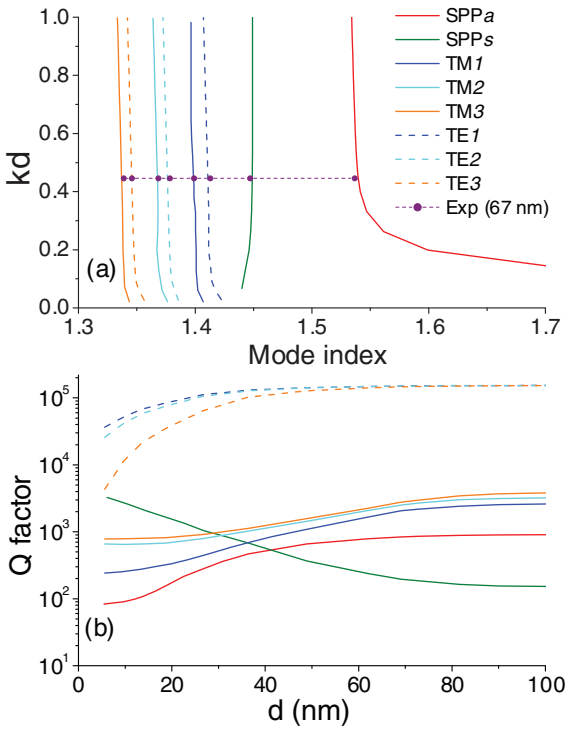

FIG. 4. (Color) (a) The dispersion relation and (b) Q factor as a function of the thickness d of silver film. The radius of fiber microcylinder is fixed at 30 μm. The other parameters are the same as in Fig. 2.

of the TE modes is approximately two orders greater than the TM modes at ∼60-nm thickness of silver film.

III. EXPERIMENTAL MEASUREMENT

As shown in Figs. 2 and 4, the mode index of a metal-coated microcavity has a large index range for the low-order modes. The ATR method can be used to measure the mode index efficiently, and has been widely used in the SPP measurement of planar metal film structure [20,22]. The ATR measurement schematic is shown in Fig. 5. Here the narrow-linewidth laser diode is used as the laser source. The output laser is polarized to TM or TE polarization by the polarizer, and is focused on the metal-coated microcylinder by a long-focus lens. The half-cylinder prism with high index is used to excite the plasmonic resonance mode. The prism is placed on the

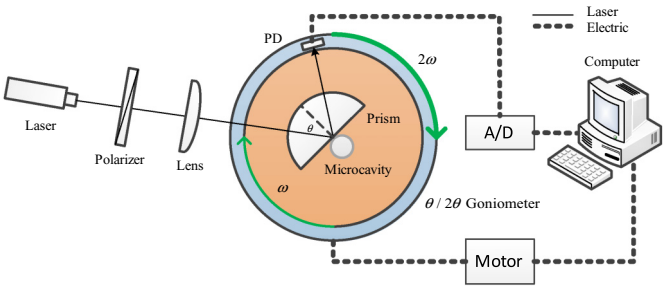

FIG. 5. (Color online) ATR experimental schematic for mode index measurement.

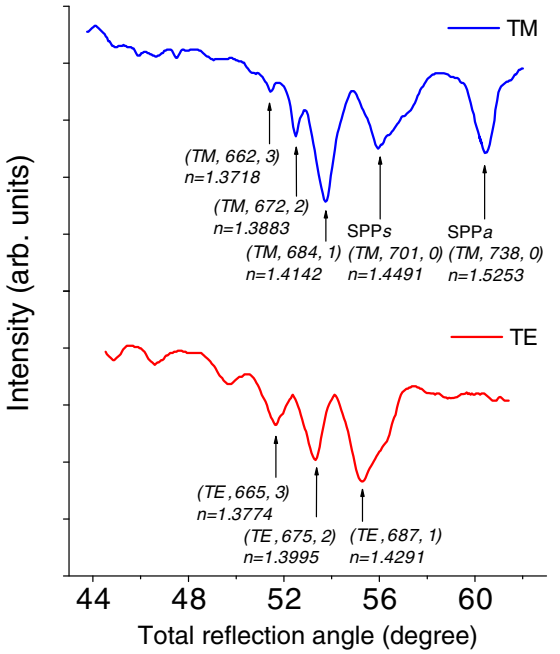

FIG. 6. (Color online) ATR spectra of silver-coated microcylinder with a 50-μm radius fiber and a 67-nm silver film. The index of the coupling prism is ∼1.75 at 650-nm wavelength.

θ motorized rotation stage of a $\theta/2\theta$ computer-controlled goniometer and the prism's axis is aligned with the rotation axis of the goniometer. The metal-coated microcylinder is attached to a glass substrate, and placed near the axis of the half-cylinder prism. Thus the focused light can be guaranteed to stay on almost the same coupling point even with large-angle rotation. Also the coupling spacing between prism and microcavity can be tuned by applying external force on the substrate. One photodiode (PD) is placed on the 2θ rotation stage to detect the reflection intensity from the rotation prism on the θ stage. The principle of the ATR measurement for mode index is that evanescent light can produce the wide-range effective index $n = n_p \sin\theta$ when the prism is rotated, where θ is the total reflection angle and n_p is the refractive index of the prism. Once the index of evanescent light is equal to that of the resonance mode, the evanescent light can be coupled into the microcavity, and the reflection light will generate the resonance dips. Thus we can measure the mode index from the position of the resonance dip.

In the experiment, the laser wavelength is fixed at 650 nm and the index of the coupling prism is ∼1.75 in this wavelength. The ATR spectra of the metal-coated microcavity with a fiber microcylinder of 50-μm radius and a silver film of 67-nm thickness are shown in Fig. 6. There are many resonance dips in the reflection intensity at certain angles, where the evanescent wave has the same index as the resonance mode. For TM polarization, the two maximal angels of the dips are at 60.65° and 55.90°, so their corresponding indexes are 1.5253 and 1.4491 for SPPa and SPPs modes, respectively. According to the theoretical results that the greater the radial mode number, the smaller the mode index, the mode indexes of TM1, TM2, and TM3 are determined from the subsequent dip angles. For TE polarization, we can get the indexes of TE l modes with

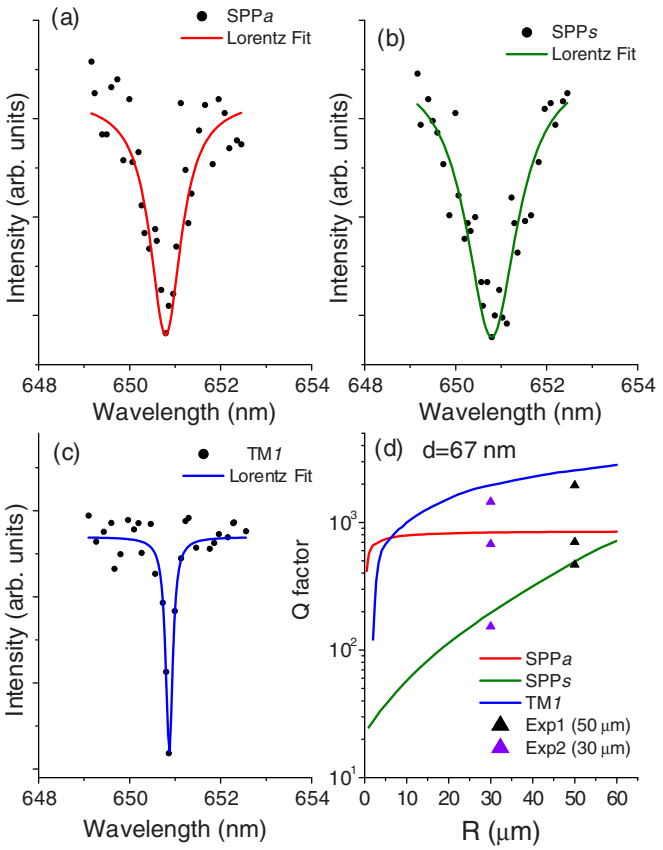

FIG. 7. (Color online) The measured resonance spectra of the mode SPPa (a), SPPs (b), and TM1 (c) of metal-coated microcylinder with a 50-μm radius fiber and a 67-nm silver film; the Q factor comparisons (d) between the theoretical and experimental values.

the same method. The measured mode indexes are shown in Fig. 6 with their corresponding modes, and also shown in Fig. 2 together with the theoretical dispersion relation for comparison. And the mode indexes are measured for another metal-coated microcylinder and shown in Figs. 2 and 4. The experimental and theoretical results agree well with each other. The measurement error is less than 1% and comes primarily from the positioning precision of resonance dips.

The Q factor of the metal-coated microcylinder is measured by the resonance linewidth method. For a metal-coated microcavity with large R, the Q factor is primarily determined by the loss of metal film. In the experiment, the resonance spectrum of the desired plasmonic WGM can be measured when the total reflection angle is fixed at the proper excitation angle of the desired mode. The measured resonance spectra and their Lorentz fits of three typical modes are measured in Fig. 7 for a metal-coated microcylinder of a 50-μm radius fiber and a 67-nm silver film. According to $Q = \lambda/\Delta\lambda$, where $\Delta\lambda$ is the full width at half maximum (FWHM) of the resonance spectrum, the Q factors of SPPa, SPPs, and TM1 modes are 702, 465, and 1950, respectively, about 16.8%, 6.4%, and 23.8% lower than their theoretical value, respectively. The measurement error of the Q factor is mainly due to the imperfections of the silver film (such as smoothness and uniformity) and the manually tunable wavelength precision of narrow-linewidth laser diode (especially for the high-Q-factor TM1 mode). As shown in Fig. 7(d), the experimental results agree well with the theoretical.

IV. CONCLUSION

We have studied the dispersion relation and Q factor of a silver-coated fiber microcylinder theoretically and experimentally. Compared with a dielectric microcavity, plasmonic WGM has some interesting characteristics in the mode index and Q factor. Two types of SPP modes, the symmetrical and asymmetrical modes, are demonstrated in the metal-coated microcavity. The Q factor of the asymmetrical SPP mode is greater than that of the symmetrical mode for small fiber radius or thick metal film. Additionally, other hybrid plasmonic WGMs have a wider mode index range and the mode index can range down to zero. Both mode index and the Q factor of plasmonic WGMs are measured in the experiments, and the experimental results agree well with the theoretical value. The studied mode characteristics can provide the theoretical foundation for its potential applications.

ACKNOWLEDGMENTS

We thank Dr. Zhenhua Ni and Wenhui Wang for help with the fabrication of the metal-coated microcavity. We also thank Dr. Zhongping Chen and Max Wiedmann for their helpful support and discussions. We gratefully acknowledge support from National Science Foundation of China (Grants No. 60907022 and No. 61205045).

[1] K. J. Vahala, Nature **424**, 839 (2003).
[2] A. B. Matsko and V. S. Ilchenko, IEEE J. Sel. Top. Quantum Electron. **12**, 1 (2006).
[3] V. S. Ilchenko and A. B. Matsko, IEEE J. Sel. Top. Quantum Electron. **12**, 15 (2006).
[4] F. Vollmer and S. Arnold, Nat. Methods **5**, 591 (2008).
[5] I. M. White, H. Oveys, and X. Fan, Opt. Lett. **31**, 1319 (2006).
[6] M. Cai, O. Painter, K. Vahala, and P. Sercel, Opt. Lett. **25**, 1430 (2000).
[7] V. Sandoghdar, F. Treussart, J. Hare, V. Lefévre-Seguin, J. M. Raimond, and S. Haroche, Phys. Rev. A **54**, R1777(R) (1996).
[8] S. Spillane, T. Kippenberg, and K. Vahala, Nature **415**, 621 (2002).
[9] T. J. Kippenberg, S. M. Spillane, and K. J. Vahala, Phys. Rev. Lett. **93**, 083904 (2004).
[10] V. S. Ilchenko, A. A. Savchenkov, A. B. Matsko, and L. Maleki, Phys. Rev. Lett. **92**, 043903 (2004).
[11] B. Min, E. Ostby, V. Sorger, E. Ulin-Avila, L. Yang, X. Zhang, and K. Vahala, Nature **457**, 455 (2009).

[12] J. Chen, Z. Li, S. Yue, and Q. Gong, Opt. Express **17**, 23603 (2009).
[13] Y.-F. Xiao, C.-L. Zou, B.-B. Li, Y. Li, C.-H. Dong, Z.-F. Han, and Q. Gong, Phys. Rev. Lett. **105**, 153902 (2010).
[14] A. Rottler, M. Harland, M. Bröll, M. Klingbeil, J. Ehlermann, and S. Mendach, Phys. Rev. Lett. **111**, 253901 (2013).
[15] A. Rottler, M. Bröll, S. Schwaiger, D. Heitmann, and S. Mendach, Opt. Lett. **36**, 1240 (2011).
[16] J. K. Kitur, V. A. Podolskiy, and M. A. Noginov, Phys. Rev. Lett. **106**, 183903 (2011).
[17] X. Zhang, Z. Ma, H. Yu, X. Guo, Y. Ma, and L. Tong, Opt. Express **19**, 3902 (2011).
[18] C. F. Bohren and D. R. Huffman, *Absorption and Scattering of Light by Small Particles* (Wiley, Berlin, 1983).
[19] I. Kaminow, W. Mammel, and H. Weber, Appl. Opt. **13**, 396 (1974).
[20] H. Li, Z. Cao, H. Lu, and Q. Shen, Appl. Phys. Lett. **83**, 2757 (2003).
[21] P. Berini, Adv. Opt. Photonics **1**, 484 (2009).
[22] H. Raether, *Surface Plasmons on Smooth and Rough Surfaces and on Gratings*, Springer Tracts in Modern Physics Vol. 111 (Springer, Berlin, 1988).